



Contents lists available at ScienceDirect

## Colloids and Surfaces A: Physicochemical and Engineering Aspects

journal homepage: [www.elsevier.com/locate/colsurfa](http://www.elsevier.com/locate/colsurfa)



# Evidence of the existence and the stability of nano-bubbles in water

Fernanda Yumi Ushikubo<sup>a</sup>, Takuro Furukawa<sup>a</sup>, Ryou Nakagawa<sup>a</sup>, Masatoshi Enari<sup>a</sup>,  
Yoshio Makino<sup>a</sup>, Yoshinori Kawagoe<sup>a</sup>, Takeo Shiina<sup>b</sup>, Seiichi Oshita<sup>a,\*</sup>

<sup>a</sup> Faculty of Agriculture, The University of Tokyo, 1-1-1, Yayoi, Bunkyo-ku, Tokyo 113-8657, Japan

<sup>b</sup> Distribution Engineering Laboratory, National Food Research Institute, 2-1-12 Kannondai, Tsukuba, Ibaraki 305-8642, Japan

### ARTICLE INFO

#### Article history:

Received 26 October 2009

Received in revised form 3 March 2010

Accepted 4 March 2010

Available online xxx

#### Keywords:

Micro-bubble

Nano-bubble

Nuclear magnetic resonance

Particle size distribution

Zeta potential

Bubble stability

### ABSTRACT

Although micro- and nano-bubble technology has been attracting attention in many fields, the state of water after the introduction of those bubbles is still not clear. In this study, the existence and stabilization of nano-bubbles after the generation of bubbles were investigated. The presence of nano-sized particles was detected through dynamic light scattering for days, when pure oxygen was used to generate the bubbles, and for less than 1 h, in the case of air bubbles. NMR spin–lattice relaxation time increased with the introduction of micro- and nano-bubbles in manganese ions solution, indicating the presence of a gas–liquid interface which adsorbed the manganese ions. Furthermore, the zeta potential measured in the water after the introduction of oxygen micro- and nano-bubbles was in the range from  $-45$  mV to  $-34$  mV and from  $-20$  mV to  $-17$  mV in water bubbled with air, indicating the presence of stable electrically charged particles. This study suggested a strong possibility of the existence of nano-bubbles in water for a long time. The stability of nano-bubbles is supported by the electrically charged liquid–gas interface, which creates repulsion forces that prevent the bubble coalescence, and by the high dissolved gas concentration in the water, which keeps a small concentration gradient between the interface and the bulk liquid.

© 2010 Elsevier B.V. All rights reserved.

## 1. Introduction

Micro- and nano-bubbles (in this study, referred to as “MNB”) present characteristics that make them special in relation to the ordinary bubbles (macro-bubbles) because of their reduced diameter size. Some of the advantages of the MNB are their high specific area (surface area per volume) and the high stagnation in the liquid phase, which increase the gas dissolution. Moreover, it was reported that when micro-bubbles collapse, free-radical generation occurs, due to the high density of ions in gas–liquid interface just before the collapse [1].

There are applications of MNB in different fields, which include the water treatment by flotation [2,3], taking advantage of the high specific area of MNB; the sterilization using ozone gas [4], which has its dissolution increased with MNB generation; contrast agent for ultrasonography [5] and the possible use in food industry for foam products, carbonated drinks and as a nutritional supplement carrier [6], in which bubble stability is desired.

Furthermore, the use of MNB in water was reported to be effective for the acceleration of metabolism in shellfishes and vegetables [7,8], as well as in aerobic cultivation of yeast [9], accelerating the

growth and increasing the yield of the products. This effectiveness, however, cannot be explained only by the increase of the dissolved oxygen (DO) concentration [8], using MNB in the solution for the hydroponic cultivation of lettuce, observed acceleration in growth in comparison with lettuce grown in solution containing similar DO concentration but without MNB. Therefore, the MNB should play an important role in the physiological activity in cells.

However, there are still many questions concerning the nano-bubbles that are not clear. Some of them are the stability and size of nano-bubbles after the introduction of MNB. This basic information is important to understand the properties of the water after the introduction of bubbles.

For this purpose, in this study, the presence of bubbles in nano-scale was investigated using dynamic light scattering (DLS). DLS is generally used to measure the size of particles such as polymers, micelles, emulsions, proteins and so on, by detecting the Brownian movement of particles.

Moreover, in order to obtain information about the electrical charge and stability of particles,  $\zeta$ -potential (zeta potential) was measured in water after the introduction of MNB.

In addition, in order to examine the existence of bubbles in water by a method based on a different physical principle than DLS, nuclear magnetic resonance (NMR) spectroscopy was used. This technique can detect weak molecular interactions such as hydrogen bonding, molecular mobility and steric effects [10], so it was

\* Corresponding author. Tel.: +81 35 841 5362; fax: +81 35 841 8174.  
E-mail address: [aoshita@mail.ecc.u-tokyo.ac.jp](mailto:aoshita@mail.ecc.u-tokyo.ac.jp) (S. Oshita).

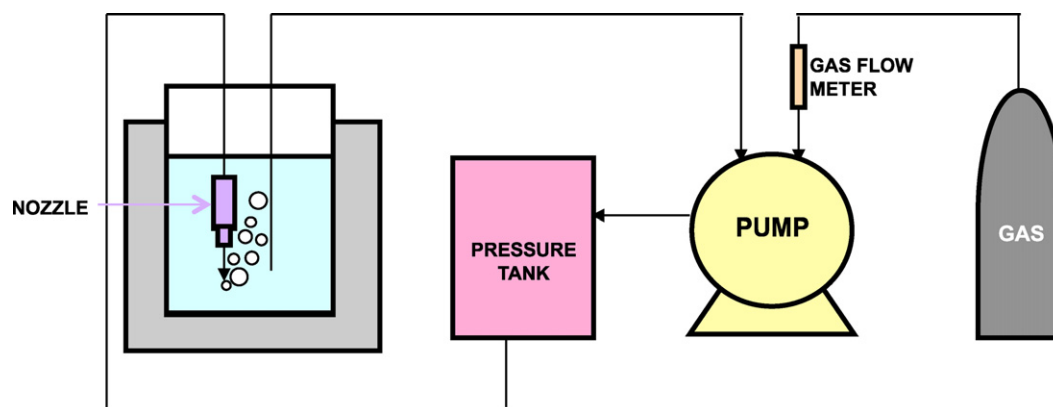


Fig. 1. Scheme of micro-bubble generator.

expected to find some modification of the intermolecular structure with the addition of MNB.

Thus, the present study aimed to investigate the stabilization of nano-bubbles in water by the measurement of particle size distribution,  $\zeta$ -potential and proton NMR spin–lattice relaxation time.

## 2. Materials and methods

### 2.1. Micro- and nano-bubbles generation

Ultrapure water was used to produce micro- and nano-bubbles. This water was obtained using a water purification system (Direct-Q, Nihon Millipore Ltd., Japan), which is equipped with a reverse osmosis cartridge and modules of ion-exchange resins and activated carbon. In the particle size distribution measurements, 2 l of ultrapure water was prepared. For the  $\zeta$ -potential measurements, 1 l of commercial ultrapure water (Kanto Chemical Co. Inc., Japan) was used, since a very strict control of water purity was required. In the case of the NMR measurements, manganese ions solution was used as a control (see Section 2.5) and the volume of solution was 1 l. The manganese ions solution was prepared using ultrapure water prepared with the Direct-Q purification system.

The main gas used to produce MNB was oxygen ( $O_2$ , purity 99.999%, Nissan Tanaka Co., Japan). For comparison reasons, air (setting a filter in the gas inlet) and xenon (Xe, purity 99.995%, Iwatani Sangyo Co. Ltd., Japan) were also used to produce MNB in some experiments.

A micro-bubble generator (OM4-GP-040, Aura Tec Co. Ltd., Japan) was used for the production of micro- and nano-bubbles (Fig. 1). In this system, the gas was introduced in the inlet part of a magnetic gear pump (MDG-R2RVA100, Iwaki Co. Ltd., Japan) while the water was suctioned. Then, the mixture of water and gas was subjected to a high pressure (0.25–0.27 MPa) in a pressurized tank to increase the dissolution of gas in the water. When the water was released under atmospheric pressure, the depressurization of the gas-supersaturated water led to the nucleation of the bubbles, which were expelled and dispersed through a nozzle at the outlet. The water was circulated in this system for 40 min at 20 °C constant temperature, controlled by a water bath (NTT-1300, Tokyo Rikakikai Co. Ltd., Japan). In this study, the water obtained after this procedure is referred to as “MNB water”, indicating the water in which micro- and nano-bubble were introduced.

According to [11], the magnetic gear pump is non-corrosive, has no seals and is free of leakage. This pump is recommended for applications in which extreme clean conditions are necessary, such as pure water processing machines and medical applications. There-

fore, the contamination of the water by the magnetic gear pump is unlikely to occur. Furthermore, in order to remove possible impurities from the equipment, three cycles of 10 min each, exchanging the water between them, were performed before the production of bubbles in the micro-bubble generator.

### 2.2. DO concentration and pH analyses

The DO (dissolved oxygen) concentration and the pH were both determined at 20 °C, using a dissolved oxygen meter (SG6, Mettler-Toledo GmbH, Switzerland) and a pH meter (D-55, Horiba Ltd., Japan), respectively.

### 2.3. Particle size distribution

The particle size distribution in nano-scale was measured using a green badge (532 nm laser) Zetasizer Nano ZS particle size analyzer (ZEN3500, Sysmex Co., Japan), which detects Brownian motion of particles through dynamic light scattering (DLS). The range of particle size which can be detected is from 0.6 nm to 6  $\mu$ m. The refractive index of the material of the “particles”, was set to 1.0, corresponding to the air. The measurements were performed at 20 °C in a glass cell with square aperture. For each sample, 5–10 replications were done.

In the particle size measurement, two different gases were used to produce MNB water: oxygen and air. Oxygen MNB water was produced at two different DO concentrations. This modification was done by the use of nozzles with different capacities to disperse the gas into the water in the outlet of the generator.

The flask containing each type of MNB water was stored at a 20 °C constant temperature room, sealed with Parafilm (Pechiney Plastic Packaging, USA). Samples were taken periodically for DLS analysis until the particle size distribution showed no repeatability.

The data was analyzed through the geometric mean diameter of the average particle size distribution. The geometric mean diameter ( $d_g$ , nm or  $\mu$ m) and the geometric standard deviation ( $S_g$ ) were calculated according to the standard ASAE S319.4 [12], as described in Eqs. (1) and (3), respectively:

$$d_g = \log^{-1} \left[ \frac{\sum_{i=1}^n (F_i \log \bar{d}_i)}{\sum_{i=1}^n F_i} \right] \quad (1)$$

$$S_{\log} = \left[ \frac{\sum_{i=1}^n F_i (\log \bar{d}_i - \log d_g)^2}{\sum_{i=1}^n F_i} \right]^{1/2} \quad (2)$$

$$S_g = \frac{1}{2} d_g [\log^{-1} S_{\log} - (\log^{-1} S_{\log})^{-1}] \quad (3)$$

where  $n$  is the number of intervals;  $F_i$  is the relative frequency of the  $i$ th interval (%);  $\bar{d}_i$  is calculated as  $(d_i \times d_{i+1})^{1/2}$  (nm or  $\mu\text{m}$ ), in which  $d_i$  is the lower size in a size interval and  $d_{i+1}$  is the upper size in a size interval of the histogram;  $S_{\log}$  is the geometric standard deviation of log-normal distribution in ten-based logarithm.

The coefficient of variation (CV), here expressed in percentage, measures the dispersion of the particle size distribution:

$$CV = \frac{S_g}{d_g} \times 100 \quad (4)$$

The particle size distribution was presented as relative frequency of particles expressed in intensity of scattered light.

#### 2.4. $\zeta$ -Potential measurement

$\zeta$ -potential measurements of the oxygen and air MNB water were performed using a Zeta Potential Analyzer (Zeecom, Microtech Co. Ltd., Japan). This system detects the electrophoretic mobility of particles and is equipped with a microscope and a CCD camera to observe the movement of particles in the range of 20 nm to 100  $\mu\text{m}$  in a 1 mm  $\times$  10 mm glass cell. The small particles can be observed by the scattering of a halogen light or laser. Fifty particles were tracked manually to determine their speed and the  $\zeta$ -potential was calculated using Smoluchowski equation.

#### 2.5. Proton NMR spin-lattice relaxation time measurement

Five replications of each sample (control and MNB) were collected in tightly closed 10 mm diameter NMR tubes, up to a 1.5 cm high liquid column. Proton spin-lattice relaxation time ( $T_1$ ) was measured in a pulsed spectrometer (JNM-MU25A, JEOL, Japan) at 25 Hz frequency and at constant temperature of 20 °C, using the saturation recovery pulse sequence.

As shown in previous study [13], the presence of oxygen in the samples was an interferer in the  $T_1$  measurements. The reason was the paramagnetic characteristic of oxygen, that is, the magnetogyric ratio of the electron in this molecule is much higher than that of a proton, which leads to a very efficient relaxation [14] and, consequently, to a decrease in  $T_1$ .

The ideal condition to perform NMR analyses would be, therefore, the complete removal of oxygen gas from the samples. However, the oxygen in the form of micro- and nano-bubble is exactly the target of this experiment. Furthermore, some difficulties were found to degas the water to a very low DO concentration. Thus, a different approach was taken in order to mask the paramagnetic effect of oxygen.

As manganese ions are paramagnetic, the addition of these ions in the water before the generation of bubbles was expected to cause an excess of paramagnetism and mask the interference of oxygen in the NMR analysis. Thus, solutions of 3, 5, 10, 15, 40 mM of manganese (II) chloride tetrahydrate ( $\text{Mn}_2\text{Cl}_4 \cdot 4\text{H}_2\text{O}$ , Kanto Chemical Co. Inc., Japan) were prepared (control sample), then oxygen MNB was produced ("O<sub>2</sub> MNB solution"). Besides, xenon MNB was generated in 10 mM manganese solution ("Xe MNB solution"). Xenon was chosen to verify the properties of MNB made by a non-paramagnetic gas. For this purpose, other gases could be used, but some factors

were considered, such as the gas solubility, which is greater than nitrogen's, for example, and because xenon is an inert gas.

In order to verify if the dissolved oxygen in the samples could affect  $T_1$ , a "O<sub>2</sub> without MNB solution" was produced and the  $T_1$  measured in this sample was compared to the O<sub>2</sub> MNB solution's value. The O<sub>2</sub> without MNB solution was prepared by the introduction of pure oxygen into a 10 mM manganese solution through a gas diffuser. This manganese solution showed DO concentration similar to the O<sub>2</sub> MNB solution at 10 mM of manganese ions and was considered to contain no MNB.

### 3. Results and discussion

#### 3.1. Particle size measurements

##### 3.1.1. Control water

The particle size distribution of the ultrapure water showed the presence of particles of geometric mean of 612 nm (CV = 130.8%). The concentration of this particles should be very low because of the irregular shape and the presence of multiple peaks in the particle size distribution. In addition, the result of the DLS measurement is given in relative frequency of particles, so the absolute concentration of particles is not provided by this method.

The detected particles were supposed to be a very few amount of air bubbles which were incorporated when the water was poured into the flask. The reason for that can be explained by the fact that Direct-Q system, which was used for the preparation of ultrapure water, can reject more than 99% of the particles, microorganisms and organic matter (molecular weight above 100 Da). Besides, no surfactants neither salts were added. Therefore, the water was expected to contain no solid particles.

After degassing the ultrapure water under vacuum for 20 min, the particle size distribution peaks were detected randomly throughout all the diameter range. Because these size distribution curves showed no repeatability, it was understood that the data were at noise level and no particles were detected. Based on these results, the ultrapure water prepared by Direct-Q system and subsequently degassed for 20 min was considered suitable as control water for the production of MNB water.

##### 3.1.2. Oxygen MNB water

Differently from the results obtained for the control water, the particle size distribution of the oxygen MNB water showed a regular shape of a mono-modal log-normal curve and the measurements had good repeatability (Fig. 2(a)). Based on this difference, there is a high possibility that the particles detected represent the diameter distribution of nano-bubbles formed by the introduction of gas.

The geometric mean of the particle size distribution was 137 nm (CV = 61.2%) just after stopping the generation of bubbles. This geometric mean oscillated slightly on the next hours until the following day (Fig. 2(b)), reaching values up to 272 nm. After three days of observation, the geometric mean diameter detected was larger (380 nm) and the variation of particles size was higher (CV = 107.4%). The larger geometric mean does not necessarily indicate that the bubbles increased in size or coalesced. The reason is that the DLS method is more sensitive to big particles than small ones, so a relative higher concentration of larger particles could have been detected. This can occur when the particle concentration is low. At a low concentration in all sizes, smaller particles can not be detected, while larger particles are still sensed. The low concentration of particles on the third day was estimated by the poor repeatability of the results shown by the error bars in Fig. 2(c) in comparison to the measurements on the previous days (Fig. 2(a) and (b)). On the third day, it seems that the particle concentration is at the limit of the minimum detection level of the particle analyzer.

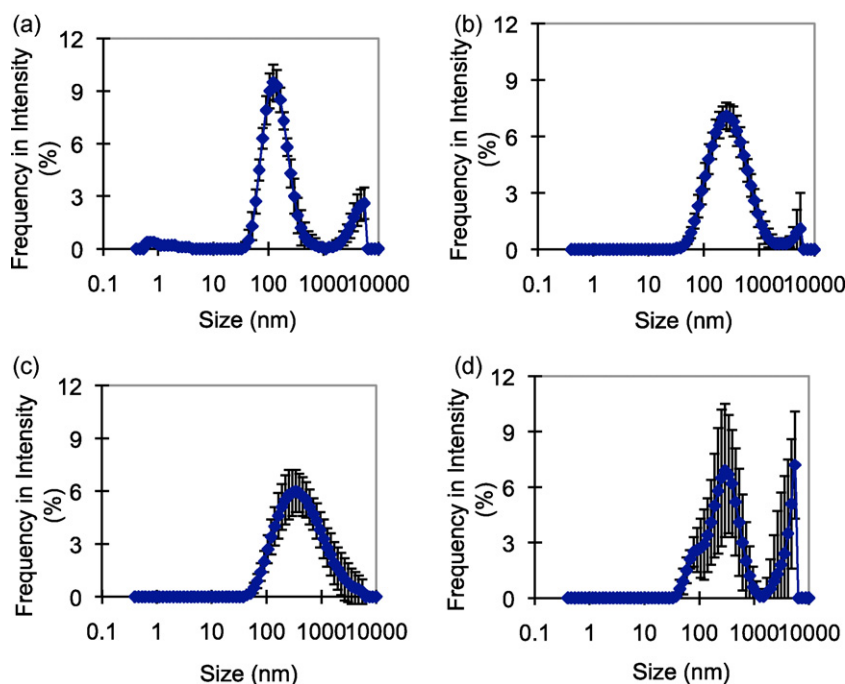


**Fig. 2.** Particle size distribution (average values,  $n = 10$ ) of oxygen MNB water (a) just after stopping the gas introduction ( $\text{DO} = 36.9 \text{ mg L}^{-1}$ ), (b) 1 day, (c) 3 days and (d) 6 days later ( $\text{DO} = 8.9 \text{ mg L}^{-1}$ ). The vertical bars represent the standard deviation of the replication data.

Finally, on the sixth day after the bubble generation, the particle size distribution curves were no longer mono-modal, the shape became irregular and there was no repeatability of the data (Fig. 2(d)). This lack of repeatability could be understood as an insufficient concentration of particles to be detected by the instrument. The decrease in concentration of particles with time is one more supporting evidence that the detected particles by DLS could be oxygen nano-bubbles.

In the literature, Kikuchi et al. [15] reported the presence of oxygen nano-bubbles after water electrolysis through the measurement of particle size by DLS. The mean particle size was 30 nm on the first day and increased to 180 nm and to 250 nm on the second and third day, respectively. After this time, the bubbles shrank until the fifth day, when no particles were observed. The range of size of the bubbles on the second and third days were similar to the results obtained in this present study, as well as the duration of the bubble detection. In other report, 290 nm air nano-bubbles were measured through DLS method after the nucleation of bubbles controlled by temperature reduction [16]. These reports in the literature and the measurements done in this present study show that the use of this technique can be reliable for measuring bubbles at nano scale, although an indirect method such as DLS is normally used for measuring solid particles.

Furthermore, in this study, the change in the particle size distribution curves with time was in accordance with the change in the DO concentration, which was at supersaturated level just after the bubble generation ( $36.9 \text{ mg L}^{-1}$ ) and at saturation level after six days ( $8.9 \text{ mg L}^{-1}$ ). The supersaturated condition could have kept a small gradient concentration of gas between the bubble interface and the bulk liquid, maintaining the bubbles stable, at a number density high enough to be detected by the laser scattering sensor. With time, the oxygen in the bubble dissolved into the water and, finally, diffused to the atmosphere. Thus, the bubble concentration decreased while the DO concentration reached the saturation level.

By the use of a nozzle with higher capacity of dispersing gas into the water, oxygen MNB water containing higher DO concentration ( $44.5 \text{ mg L}^{-1}$ ) was produced. The particle size distribution was similar as the previous experiment at lower DO concen-

tration: mono-modal log-normal curves with good repeatability. The geometric mean diameter was also in similar range of size (125 ~ 172 nm) and the dispersion of the particle size was small ( $\text{CV} = 55.4\% \sim 72.6\%$ ). However, at a higher initial DO concentration, particles were observed for a longer time, as bubbles were detected until the fifteenth day after the MNB water production. Only on the eighteenth day, non-uniform and very scattered curves were obtained. The DO concentration of the MNB water became near the saturation condition on the fifth day ( $10.3 \text{ mg L}^{-1}$ ). On the eighteenth day, the DO concentration had reached to the saturation equilibrium at  $9.1 \text{ mg L}^{-1}$ .

Based on the data obtained, it was observed that the higher initial DO concentration could extend the particle stability. This corroborates with the possibility of the existence of nano-bubbles, since at higher DO concentration, the oxygen diffusion time would take more time. However, only the high DO concentration cannot explain the extension of the nano-bubble stability. From the fifth day after the bubble generation, although the DO concentration was near the saturation condition, the particle size distribution could still indicate clearly the presence of nano-particles. Therefore, there should be other factors which can contribute to the stabilization of nano-bubbles besides the high gas concentration in the liquid.

### 3.1.3. Air MNB water

When air was introduced in water instead of oxygen, the repeatability of data was not as good as that obtained for oxygen MNB water and the shapes of the distribution curves were irregular. The geometric mean of the particle size distribution fluctuated from 350 nm in the first 5 min to 140 nm after 25 min after the bubble generation. The dispersion of data was larger (107.3% at 5 min and 137.5% at 25 min) than that obtained in  $\text{O}_2$  MNB water. Some particles could still be detected 45 min after the bubble generation at the size of 205 nm ( $\text{CV} = 120.7\%$ ), but at 70 min, the particles could not be detected. The DO concentration just after the air bubble generation was  $11.7 \text{ mg L}^{-1}$  and was kept stable until the last observation time.

The poor repeatability and the irregular distribution curves of air MNB water indicate that the concentration of particles should be

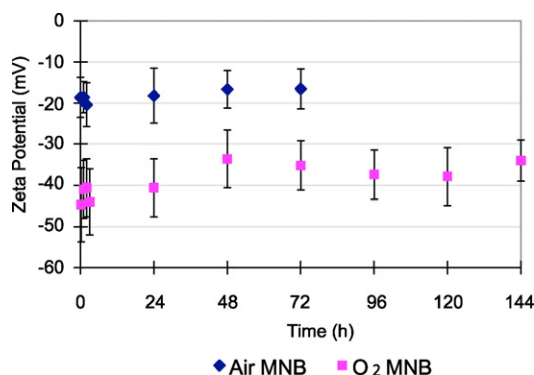


**Fig. 3.** Average values of  $\zeta$ -potential measurements in O<sub>2</sub> MNB water and air MNB water with time ( $n = 50$ ). The vertical bars show the standard deviation of the measurements.

under the minimum detection level to obtain more accurate data. The results suggest the low stability of air MNB compared to the oxygen MNB, since the concentration of air bubbles should be much lower than that of oxygen MNB.

The big difference between the periods in which bubbles could be observed stable in the oxygen MNB water (3 or 15 days) and in the air MNB water (less than 1 h) should be related to the lower dissolution of the air in water in relation to the dissolution of oxygen. At a lower concentration of dissolved gas in the water, the concentration gradient across the gas–liquid interface of the bubble is higher, which leads to a more efficient gas transfer to the liquid phase.

### 3.2. $\zeta$ -Potential

The measurement of  $\zeta$ -potential in O<sub>2</sub> MNB and air MNB water with time showed negative values (Fig. 3). Moreover, the average of absolute values of O<sub>2</sub> MNB water (34–45 mV) were higher than those of air MNB water (17–20 mV). The pH of the O<sub>2</sub> MNB water was between 6.2 and 6.4 and that of the air MNB water was in the range of 5.7 and 6.2.

In the literature, Graciaa et al. [17] reported a  $\zeta$ -potential of  $-65$  mV in air bubbles formed in deionized water, while Takahashi [18] obtained  $-35$  mV in distilled water (pH 5.8). According to Graciaa et al. [19], the disparity in results in the literature is due to the differences in the purification methods of the water. However, in both reports, as well in this present study, the value of  $\zeta$ -potential was negative. The negative value is attributed to the predominance of hydroxide ions in the first molecular layers of water at the gas–liquid interface [20].

According to Spanos et al. [21], the absolute  $\zeta$ -potential value normally taken as a minimum to observe a potential stability is 30 mV. At a high absolute  $\zeta$ -potential, the electrical charged particles tend to repel each other, avoiding aggregation of particles in a colloidal dispersion. In the case of a bubble dispersion, the high  $\zeta$ -potential could create repulsion forces that would avoid the coalescence of bubbles and contribute to the stabilization of the

bubbles. Therefore, in this study, the O<sub>2</sub> MNB could be stabilized in water by the electrically charged surfaces, while the air MNB would be below the limit of the stabilization by repulsion forces.

Furthermore, it was observed a relation between  $\zeta$ -potential and DO concentration. In the measurements performed in O<sub>2</sub> MNB water until the first day after the bubble production,  $\zeta$ -potential presented absolute values in the range from 40 mV to 45 mV. During this period, the DO concentration was above the saturation level: 40.8 mg L<sup>-1</sup> just after the bubble generation and 14.9 mg L<sup>-1</sup> one day later. From the second day after the bubble generation, when the DO concentration reached 10.3 mg L<sup>-1</sup> and tended to stabilize near the saturation level (9.1 mg L<sup>-1</sup> at 20 °C), the  $\zeta$ -potential absolute value was lower and was practically constant in the range from 34 mV to 38 mV.

In air MNB water,  $\zeta$ -potential, as well as the DO concentration did not vary much with time. The DO concentration was 10.7 mg L<sup>-1</sup> just after the bubble production, decreasing to 10.0 mg L<sup>-1</sup> in the first hour after stopping the bubble generation and stabilizing at saturation level in the next hour.

One important point to observe is that, during the measurements of the particle mobility, although the velocity of the particles did not seem to vary with time (resulting in practically constant  $\zeta$ -potential), the amount of particles did. Therefore, while the charge of the particles practically did not change, the concentration of particles or bubbles should be decreasing with time (qualitative data). For example, in the case of air MNB water, the concentration of particles after 3 days of the bubble generation became so low that the  $\zeta$ -potential measurements could not be continued.

In summary, the  $\zeta$ -potential measurements showed that the MNB water is negatively charged and that the O<sub>2</sub> MNB water presented higher electrical charge than the air MNB water. The high value of  $\zeta$ -potential can be related to the stability of bubbles, explained by the repulsion forces generated by the electrically charged surfaces of bubbles, which avoid the bubble coalescence.

### 3.3. Proton NMR spin–lattice relaxation time ( $T_1$ )

After the introduction of oxygen as micro- and nano-bubbles in the manganese ions solution, it was verified that  $T_1$  increased ( $p < 0.05$ ) in all the manganese concentrations tested, as shown in Table 1.

The pH value seemed to increase very slightly with the introduction of oxygen, probably because of the release of the naturally dissolved carbon dioxide from the solution due to the gas bubbling.

One important point is that the increase in  $T_1$  was caused by the production of MNB, but not by the increase in DO concentration. A more detailed examination in the case of 10 mM Mn<sup>2+</sup> solutions is shown in Fig. 4.

The O<sub>2</sub> without MNB solution at 10 mM Mn<sup>2+</sup> concentration has similar DO concentration as the O<sub>2</sub> MNB solution: 37.1 mg L<sup>-1</sup> and 38.8 mg L<sup>-1</sup>, respectively. However, the  $T_1$  of O<sub>2</sub> without MNB solution did not differ statistically from the control sample ( $p < 0.05$ ). Therefore, the generation of micro- and nano-bubbles is the only reason for the  $T_1$  increase observed in O<sub>2</sub> MNB solution. In other

**Table 1**

$T_1$ , DO concentration and pH of Mn<sup>2+</sup> solution at different concentrations, before (control) and after introduction of oxygen micro- and nano-bubbles (O<sub>2</sub> MNB).

[Mn <sup>2+</sup> ] (mM)	Control			O <sub>2</sub> MNB		
	$T_1$ (ms)	DO (mg L <sup>-1</sup> )	pH	$T_1$ (ms)	DO (mg L <sup>-1</sup> )	pH
3	36.7±0.1 <sup>a</sup>	7.7	5.97	37.60±0.06 <sup>b</sup>	39.6	6.30
5	20.8±0.1 <sup>a</sup>	8.0	5.80	21.35±0.06 <sup>b</sup>	39.1	6.12
10	11.57±0.03 <sup>a</sup>	8.6	5.59	12.48±0.06 <sup>b</sup>	38.8	5.71
15	7.77±0.03 <sup>a</sup>	9.4	5.78	8.18±0.03 <sup>b</sup>	39.6	5.83
40	2.894±0.004 <sup>a</sup>	8.5	5.88	3.01±0.02 <sup>b</sup>	35.8	5.69

Different superscript letter means that the  $T_1$  of control and O<sub>2</sub>MNB samples differ significantly ( $p < 0.05$ ).

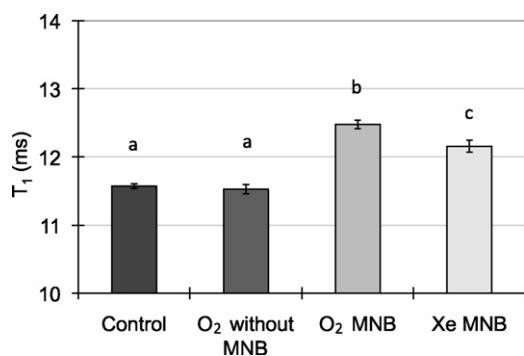


Fig. 4.  $T_1$  value of 10 mM  $Mn^{2+}$  solutions: control,  $O_2$  without MNB solution,  $O_2$  MNB solution and Xe MNB solution. Different letters means that the samples differ significantly between each other ( $p < 0.05$ ).

words, the difference between the  $T_1$  values of  $O_2$  without MNB and  $O_2$  MNB solutions indicates that the paramagnetic effect of oxygen was successfully masked by the manganese ions.

Moreover, it was observed that the Xe MNB solution indicated the same tendency of increasing  $T_1$  as that observed in the  $O_2$  MNB solution (Fig. 4). Similarly, in this case, the  $T_1$  values were independent of the DO concentration, which were  $38.8 \text{ mg L}^{-1}$  in  $O_2$  MNB solution and  $0.5 \text{ mg L}^{-1}$  in Xe MNB solution. Furthermore, it seems that the presence of MNB itself is more decisive for the dynamic state of the solution than the type of gas that composes the bubbles.

In a previous study, Oshita et al. [22] reported the shortening of  $T_1$  when xenon gas was applied to distilled water under high pressure. The authors related this result to the increase in the viscosity of water after it was subjected to the xenon gas. The change in viscosity was caused by the formation of “structured water” as a result of the application of xenon under high pressure.

On the other hand, the opposite tendency was observed in this present study, with the  $T_1$  increase after Xe MNB production. This opposite result could be explained by the difference of structures formed when xenon gas is applied under high pressure and when introduced as micro- and nano-bubbles. The “structured water” was not detected in this case.

One major possible reason for the relaxation time change in Xe and  $O_2$  MNB solutions could be the change in apparent concentration of manganese ions. As bubble surfaces are negatively charged (see Section 3.2), some amount of manganese ions should adsorb on the bubble surface, resulting in a lower apparent  $Mn^{2+}$  concentration in the solution. Since the paramagnetic material decreases  $T_1$  only when it directly contacts with a water molecule, the lower apparent concentration of  $Mn^{2+}$  of the solution induced a lower paramagnetic effect. As a consequence, a longer  $T_1$  was observed in solutions containing MNB.

In short, it was verified that the increase in  $T_1$  with the introduction of MNB was caused by the presence of bubbles. From a different approach, the existence of nano-bubbles in water was suggested through NMR spectroscopy.

#### 3.4. Discussion about the stabilization of nano-bubbles

In micro-scale, bubbles tend to shrink under the water until they collapse, as the inner pressure increases [23]. The Young–Laplace equation describes the relation between the pressure difference and the radius of the bubble:

$$P = P_l + 2 \frac{\sigma}{r} \quad (5)$$

in which  $P$  is the gas pressure,  $P_l$  is the liquid pressure,  $\sigma$  is the surface tension and  $r$  is the bubble radius.

According to Eq. (5), nano-bubbles should not exist at stable condition under atmospheric pressure, because of the very high internal pressure. A bubble of 100 nm radius, for example, should have an internal pressure of approximately 0.15 MPa (using  $\sigma = 0.072785 \text{ N m}^{-1}$ , [24]). At this high pressure, nano-bubbles should collapse in a very short time. Ljunggren and Eriksson [25], through calculations based on the mass transfer of the gas at the bubble interface to the bulk liquid, and considering the Young–Laplace equation, found that the lifetime of a 100 nm radius gas bubbles would be 100  $\mu\text{s}$ .

Moreover, Matsumoto and Tanaka [26], when verifying the validity of Eq. (5) for nano-bubbles using molecular dynamics simulation, found out that the surface tension and the vapor pressure were practically constant, independently of the bubble size. They concluded that the condition for the nano-bubble to exist obeying Eq. (5) is that the liquid phase should be under a large vacuum or high tensile stress. Therefore, according to this study, the nano-bubbles should not be in equilibrium state under atmospheric pressure.

However, the validity of Eq. (5) for nano-bubbles is not a consensus in the literature. According to Hemmingsen [27], it may not be applicable considering a constant surface tension of the liquid, since the surface tension is greatly affected by the interface curvature and the internal gas pressure at nano scale. In addition, Tolman [28] calculated theoretically that the surface tension in drops should decrease significantly at small sizes. That is, the surface tension changes with the curvature at the gas–liquid interface. A lower surface tension at the nano-bubble interface would result in a lower internal pressure, which could contribute to the stabilization of the bubbles.

In agreement with the hypothesis of a lower internal pressure of nano-bubbles, [29], based on molecular simulation data, concluded that there are too few vapor atoms inside nano-bubbles, so the interior gas pressure would not be high enough to support the force balance of a nano-bubble. The authors stated that the internal pressure should be much lower than predicted by Eq. (5), so it should not be valid for nano-bubbles. Instead, the liquid–gas interface should play an important role in the stabilization of nano-bubbles.

In this study, some evidence of the existence of nano-bubbles was found experimentally. The particle size distribution curves were very clear after the production of bubbles and remained stable on the following measurements. After a period, the distribution curve became fluctuated, which would indicate the disappearance of bubbles. If those particles were not bubbles but some solid particles, the particle size distribution should not fluctuate with time. Moreover, the increase in  $T_1$  could be an indication of the presence of bubbles, which led to the adsorption of manganese ions on their surface.

Therefore, there should be some mechanism that explain the stabilization of the bubbles at nano scale. One factor observed in this study was the gas supersaturation condition of the water, which can reduce the gas transfer rate from the bubble to the liquid. However, this factor should be not the only one that can explain the nano-bubble stability, since nano-bubbles should exist even near or after reaching the saturation equilibrium. Other contribution to the nano-bubble should be related to the electrical charge at the bubble surface, as indicated by the  $\zeta$ -potential measurements. The high absolute value of  $\zeta$ -potential could avoid the bubble coalescence by the creation of repulsion forces, as discussed in Section 3.2.

The existence of nano-bubbles in saturated liquids was also reported by Bunkin et al. [30,31], who justify the stability of the bubbles by the adsorption of ions on their surface, which makes Coulomb repulsion forces compensate surface tension forces. In the later report, the authors concluded that 70–90 nm radii air bubbles are gathered in micro-scale clusters in pure water.

Furthermore, the negative  $\zeta$ -potential was related to the hydrogen bond network at the gas–liquid interface that has a different structure from that of the bulk water [18]. The change in the hydrogen bond is also described by Ohgaki et al. [32], in which a “hard hydrogen bond” at the gas–liquid interface, detected by infrared spectroscopy is reported. The change in the water structure at the interface could be a hint to explain the stabilization of nanobubbles. This hypothesis can be related to the study of Nagayama et al. [29] about the bubble interface, which should have some role in keeping the nano-bubbles stable at a low internal pressure, as discussed above.

#### 4. Conclusion

This study confirmed experimentally and with good precision the existence of nano-bubbles in water by the particle size distribution,  $\zeta$ -potential and proton spin–lattice relaxation time ( $T_1$ ) measurements. The particle size distribution measured by DLS method indicated the presence of particles with a few hundreds nanometers in diameter. These particles showed a good repeatability during a period after the bubble production. This period varied from less than 1 h, in the case of air bubbles, to some days, in the case of oxygen bubbles. The particle size distribution fluctuated after this period and lost the repeatability. This fact is thought to be one evidence of nano-bubbles existence and their subsequent disappearance. The stability of nano-sized bubbles was explained by both the high dissolved gas concentration in water and the electrically charged interface of the bubbles. The latter reason was supported by the  $\zeta$ -potential measurements, in which the high absolute  $\zeta$ -potential obtained in  $O_2$  MNB water could have avoided the coalescence of bubbles, while in air MNB water the absolute  $\zeta$ -potential was not high enough. The presence of electrical charges could be related to some special water structure at the interface, which promotes the stabilization of the nano-bubbles. Moreover, the change in  $T_1$  of  $Mn^{2+}$  solution after the introduction of oxygen MNB could be one more evidence of the existence of electrically charged bubbles, suggested by the adsorption of  $Mn^{2+}$  on the bubble surface.

#### Acknowledgments

The authors express their appreciation for the technical assistance given by Sysmex Co. (Japan) and for the financial support by the Food Nanotechnology Project of the Ministry of Agriculture, Forestry and Fisheries of Japan and by Grant-in-Aid for Exploratory Research (19658091). They are also grateful to the former professor Hisashi Uedaira at Hokkaido University, External Director Toshio Ishii at Kyowa Interface Science Co., Ltd., and Prof. Kenichi Yoshikawa at Kyoto University for the stimulating discussion about the interpretation of the data of proton NMR relaxation time of  $Mn^{2+}$  solution with and without bubbles.

#### References

- [1] M. Takahashi, K. Chiba, P. Li, Free-radical generation from collapsing microbubbles in the absence of a dynamic stimulus, *The Journal of Physical Chemistry B* 111 (6) (2007) 1343–1347.
- [2] S.E. Burns, S. Yiacoumi, C. Tsouris, Microbubble generation for environmental and industrial separations, *Separation and Purification Technology* 11 (3) (1997) 221–232.
- [3] P. Li, H. Tsuge, Water treatment by induced air flotation using microbubbles, *Journal of Chemical Engineering of Japan* 39 (8) (2006) 896–903.
- [4] P. Li, H. Tsuge, Ozone transfer in a new gas-induced contactor with microbubbles, *Journal of Chemical Engineering of Japan* 39 (11) (2006) 1213–1220.
- [5] M.J.K. Blomley, J.C. Cooke, E.C. Unger, M.J. Monaghan, D.O. Cosgrove, Microbubble contrast agents: a new era in ultrasound, *British Medical Journal* 322 (2007) 1222–1225.
- [6] Y. Shen, M.L. Longo, R.L. Powell, Stability and rheological behavior of concentrated monodisperse food emulsifier coated microbubble suspensions, *Journal of Colloid and Interface Science* 327 (1) (2008) 204–210.
- [7] H. Onari, Fisheries experiments of cultivated shells using micro-bubbles techniques, *Journal of Heat Transfer Society of Japan* 40 (160) (2001) 2–7 (in Japanese).
- [8] J. Park, K. Kurata, Application of microbubbles to hydroponics solution promotes lettuce growth, *Hort Technology* 19 (1) (2009) 212–215.
- [9] K. Ago, K. Nagasawa, J. Takita, R. Itano, N. Morii, K. Matsuda, K. Takahashi, Development of an aerobic cultivation system by using a microbubble aeration technology, *Journal of Chemical Engineering of Japan* 38 (9) (2005) 757–762.
- [10] M. Balci, Basic  $^1H$ - and  $^{13}C$ -NMR Spectroscopy (Chapter 10): Absorption and Resonance, Elsevier, Amsterdam, Netherlands, 2005, pp. 274–251.
- [11] ASABE, ASABE Standards 2009. Standard Engineering Practices Data, chap. ASAE S318.4. Method of Determining and Expressing Fineness of Feed Materials by Sieving, 56th edn., ASABE, St. Joseph, USA, 2009.
- [12] ASABE, ASABE Standards 2009. Standard Engineering Practices Data, chap. ASAE S318.4. Method of Determining and Expressing Fineness of Feed Materials by Sieving, 56th edn., ASABE, St. Joseph, USA, 2009.
- [13] F.Y. Ushikubo, S. Oshita, T. Furukawa, Y. Makino, Y. Kawagoe, T. Shiina, A study of water containing micro and nano-bubbles and its possible effect on physiological activity, in: *Proceedings of International Conference of Agricultural Engineering*, Iguassu Falls City, Brazil, August–September, 2008.
- [14] R.J. Abraham, J. Fisher, P. Loftus, *Introduction to NMR Spectroscopy*, John Wiley and Sons, Chichester, England, 1988.
- [15] K. Kikuchi, A. Ioka, T. Oku, Y. Tanaka, Y. Saihara, Z. Ogumi, Concentration determination of oxygen nanobubbles in electrolyzed water, *Journal of Colloid and Interface Science* 329 (2) (2009) 306–309.
- [16] A.S. Najafi, J. Drelich, A. Yeung, Z. Xu, J. Masliyah, A novel method of measuring electrophoretic mobility of gas bubbles, *Journal of Colloid and Interface Science* 308 (2) (2007) 344–350.
- [17] A. Graciaa, G. Morel, P. Saulner, J. Lachaise, R.S. Schechter, The zeta-potential of gas bubbles, *Journal of Colloid and Interface Science* 172 (1995) 131–136.
- [18] M. Takahashi, Zeta potential of microbubbles in aqueous solutions: electrical properties of the gas–water interface, *Journal of Physical Chemistry B* 190 (46) (2005) 21858–21864.
- [19] A. Graciaa, P. Creux, J. Lachaise, *Encyclopedia of Surface and Colloid Science*, vol. 2, chap. Electrokinetics of bubbles, Marcel Dekker, New York, 2002. 1876–1886.
- [20] G.K. Kelsall, S. Tang, S. Yurdakul, A.L. Smith, Electrophoretic behaviour of bubbles in aqueous electrolytes, *Journal of Chemical Society, Faraday Transactions* 92 (1996) 3887–3893.
- [21] N. Spanos, P.G. Klepetsanis, P.G. Koutsoukos, *Encyclopedia of Surface and Colloid Science*, vol. 1, chap. Calculation of Zeta-potentials from Electrokinetic Data, Marcel Dekker, New York, 2002, pp. 829–845.
- [22] S. Oshita, Y. Seo, Y. Kawagoe, Relaxation Time of Protons in Intracellular Water of Broccoli, *Agricultural Engineering International: The CIGR E-Journal* vol. 1, uRL: <http://www.cigrjournal.org/index.php/Ejournal/article/viewFile/1040/1033> (last accessed 09.02.10).
- [23] M. Takahashi, T. Kawamura, Y. Yamamoto, H. Onari, S. Himuro, H. Shakutsui, Effect of shrinking microbubble on gas hydrate formation, *The Journal of Physical Chemistry B* 107 (10) (2003) 2171–2173.
- [24] F.J. Millero, *The Physical Chemistry of Natural Waters*, Wiley-Interscience, New York, 2001.
- [25] S. Ljunggren, J.C. Eriksson, The lifetime of a colloid-sized gas bubble in water and the cause of hydrophobic attraction, *Colloids and Surfaces A: Physicochemical and Engineering Aspects* 129–130 (1997) 151–155.
- [26] M. Matsumoto, K. Tanaka, Nano bubble–size dependence of surface tension and inside pressure, *Fluid Dynamics Research* 40 (7–8) (2008) 546–553.
- [27] E.A. Hemmingsen, *Encyclopedia of Surface and Colloid Science*, vol. 4, chap. Spontaneous Gas Bubble Formation in Water, Marcel Dekker, New York, 2002, pp. 4775–4784.
- [28] R.C. Tolman, The effect of droplet size on surface tension, *The Journal of Chemical Physics* 17 (3) (1949) 333–337.
- [29] G. Nagayama, T. Tsuruta, P. Cheng, Molecular dynamics simulation on bubble formation in a nanochannel, *International Journal of Heat and Mass Transfer* 49 (23–24) (2006) 4437–4443.
- [30] N.F. Bunkin, K.V. Indukaev, P.S. Ignat'ev, Spontaneous self-organization of microbubbles in a liquid, *Journal of Experimental and Theoretical Physics* 104 (3) (2007) 486–498.
- [31] N.F. Bunkin, N.V. Suyazov, A.V. Shkirin, P.S. Ignat'ev, K.V. Indukaev, Study of nanostructure of highly purified water by measuring scattering matrix elements of laser radiation, *Physics of Wave Phenomena* 16 (4) (2008) 243–260.
- [32] K. Ohgaki, N.Q. Khan, Y. Joden, A. Tsuji, T. Nakagawa, Physicochemical approach to nanobubbles solution, *Chemical Engineering Science* 65 (3) (2010) 1296–1300.